Two Cooling Approaches of an Electrohydraulic Energy Converter For Non-Road Mobile Machinery

Pia Lindh, *Senior Member, IEEE*, Jonna Tiainen, Aki Grönman, Teemu Turunen-Saaresti, Chong Di, *Member, IEEE*, Lasse Laurila, Eero Scherman, Heikki Handroos, *Member, IEEE*, and Juha Pyrhönen, *Senior Member, IEEE*

***Abstract*—The energy efficiency of non-road mobile machinery can be improved by using e.g., an electric drive system as a servo controller of a hydraulic machine to get an efficient electrohydraulic (EH) converter. However, the cooling of EH devices require more understanding and new innovations. This work presents a design of a 7-kW integrated EH machine and studies its electric motor heat transfer phenomena both experimentally and numerically. Further, to better match the torque and speed performances of the permanent magnet synchronous motor (PMSM) and the hydraulic machine a planetary step-down gear is utilized to triple the output torque of the PMSM. The integrated motor and gear system is then connected to a bent axis piston hydraulic machine, which is capable of operating both as a motor and a pump. Two different electric motor cooling approaches are investigated. The first cooling approach is to use some hydraulic oil inside the motor-gear chamber to let it flow freely as a result of the rotor rotation and move the losses to the surface of the converter cover, which is equipped with some air cooling fins. In the second approach, the oil flows through the converter and removes the losses more effectively. Motor losses and thermal behaviour are studied within these two cooling approaches. Computational fluid dynamic (CFD) simulations are performed to find how the coolant is distributed inside the machine and how heat is distributed in the device.**

***Index Terms*—Computational fluid dynamics, electrical machine, oil-cooling, permanent magnet machine.**

Manuscript received 1 March 2022; revised 18 May 2022 and 29 July 2022; accepted 31 August 2022. Date of publication 20 September 2022; date of current version 19 January 2023. Paper 2022-EMC-0227.R2, presented at the 2021 IEEE International Electric Machines & Drives Conference, Hartford, CT, USA, May 17–20, and approved for publication in the IEEE TRANSACTIONS ON INDUSTRY APPLICATIONS by the Electric Machines Committee of the IEEE Industry Applications Society. This work was supported by the INERCOM Project. *(Corresponding author: Pia Lindh.)*

Pia Lindh, Lasse Laurila, and Juha Pyrhönen are with the LUT School of Energy Systems, Laboratory of Electrical Drives Technology, LUT University, 53850 Lappeenranta, Finland (e-mail: pia.lindh@lut.fi; lasse.laurila@lut.fi; juha.pyrhonen@lut.fi).

Jonna Tiainen, Aki Grönman, and Teemu Turunen-Saaresti are with the LUT School of Energy Systems, Laboratory of Fluid dynamics, LUT University, 53850 Lappeenranta, Finland (e-mail: jonna.tiainen@lut.fi; aki.gronman@lut.fi; teemu.turunen-saaresti@lut.fi).

Heikki Handroos is with the LUT School of Energy Systems, Mechanical Engineering, LUT University, 53850 Lappeenranta, Finland (e-mail: heikki.handroos@lut.fi).

Chong Di is with the Electrical Drives, Hefei University of Technology, Hefei, China (e-mail: chong.di@hfut.edu.cn).

Eero Scherman is with the LAB University of Applied Sciences, Technology, 53850 Lappeenranta, Finland (e-mail: eero.scherman@lab.fi).

Color versions of one or more figures in this article are available at https://doi.org/10.1109/TIA.2022.3207983.

Digital Object Identifier 10.1109/TIA.2022.3207983

I. INTRODUCTION

THE improvement of mobile machinery's energy efficiency requires new innovations. Hydraulics is important e.g., in non-road systems which need to cut their carbon emissions by 90% by 2050 [1]. Further, the latest emission regulations encourage hybridization and electrification [1], which are of critical importance in reducing the sector's greenhouse gas emissions. The target of this research is to design an integrated electric motor-gear system for an EH energy converter for different applications e.g., in hybrid non-road mobile machinery like excavators, loaders, harvesters, etc … In this research, the non-road mobile machine used as an example is a log loader, and its required power cycles are measured to analyse energy saving potential.

The benefits of hybridisation, in general, are system efficiency increase, lower fuel consumption, lower pollution, and energy-saving by regeneration [2], [3], [4]. Earlier studies have proven that in some log-loader cycles energy savings can be as high as 50% [5]. In non-road mobile machinery, there is recent interest in integrating a hydraulic pump with an electric motor to gain better performance e.g., in [6] a 1.1-kW linear motor is integrated into a pump with a liquid flow of 25 L/min. Another study [7] investigates an electric-hydraulic converter for a 20-ton excavator applying a high-speed approach with liquid cooling. This study also reveals that axial-flux machine PMSM topologies can offer higher flow ramp rates than radial-flux machines. Recent research on the dynamic behaviour of combining an electric motor with a hydraulic pump is described in [8] and research on failure situations and protection in [9].

The designed EH converter has an outer rotor permanent magnet synchronous machine integrated with a planetary gear and a hydraulic machine. The electric machine is designed to have a low active material volume and therefore its stator and rotor are placed around the planetary gear. Such an arrangement brings the torque-producing air gap on the highest possible radius enabling high torque capability per mass.

The hydraulic machine delivers hydraulic oil to drive a cylinder or works as a motor to convert the kinetic or potential energy of the hydraulic system back to mechanical and finally to electrical energy. With this converter, the volumetric flow rate of oil is adjusted directly by adjusting the rotation of the electric machine by a power electronic converter instead of having a high loss throttling control system by conventional valves. In many cases, the working hydraulics of the actuator are supplied via

long hoses, pipes, and throttling valves by a centralized hydraulic pump. Such pipes and hoses may cause 30% pressure losses, another 24% of losses are caused by valves, and finally 20% more by the pump [10]. Except for pump losses, these losses can be effectively mitigated by using electrically distributed energy and decentralized electrohydraulic actuators.

There are various motor cooling options available from passive cooling, forced air cooling, combined special cooling, and liquid cooling [11], [12]. In this study, two cooling approaches are compared:

1) Immersion cooling (without external cooling circuits). In this case, hydraulic oil, available anyway in the system, is used as a medium transferring heat to the outer surfaces of the converter from where the losses are dissipated towards ambient.
2) Oil flow cooling: 1 bar, 33 °C oil is pumped towards end windings (Drive End). Most oil drops flow to a channel between the rotor and casing. Part of oil flows axially via the air gap. The cooling-oil circuit consists of a pump, an oil cooler, an oil tank, and a flow meter with sensors.

Immersion cooling is a safe and easily implemented method to remove heat from the inner machine to its outer cover, however, the maximum allowable oil temperature is restricting the use. Permanent magnets (N48SH) can sustain max 150 °C, copper windings and their insulations can sustain 155 °C, but most hydraulic oils can tolerate only 90 °C. Therefore, to reach the highest possible power from a device the oil temperature must be controlled, and in practice, oil must be cooled.

II. Combined Electric Motor, Planetary Gear and Pump

A 7-kW radial-flux outer-rotor PM prototype machine with 24 slots and 20 poles was designed and constructed. The electric motor stator is surrounding the planetary gear to reach a small volume. Permanent magnet synchronous machines (PMSMs) especially as outer rotor versions enable high specific torque, and consequently, this machine type was selected for the EH converter prime mover. The PMSM-gear-pump system is dedicated to powering a log loader boom lifting logs with maximum mass of 650 kg and max lifting distance of 6 m. The load cycles (torque and speed as a function of time) of the log loader were recorded and utilized as boundary conditions for the design of the converter. Its electric motor is designed for periodic duty [13]. A log loader cycle including lifting, carry-over and lowering is close to the electric drive duty type S7, which is defined as a sequence of identical duty cycles, each cycle consisting of a starting time, time of operation at constant load and a time of electric braking. Periodic load cycle S3 emulates well the log loader's lifting phase: a sequence of identical duty cycles including a constant load time and rest time. An industrial planetary gear and a fixed displacement bent axis piston hydraulic machine were selected to meet the boundaries: max pressure 200 bars, hydraulic machine displacement 19 cm^3/rev, gear ratio 1:3, hydraulic machine max speed 2000 r/min, and nominal flow 34.2 L/min [11].

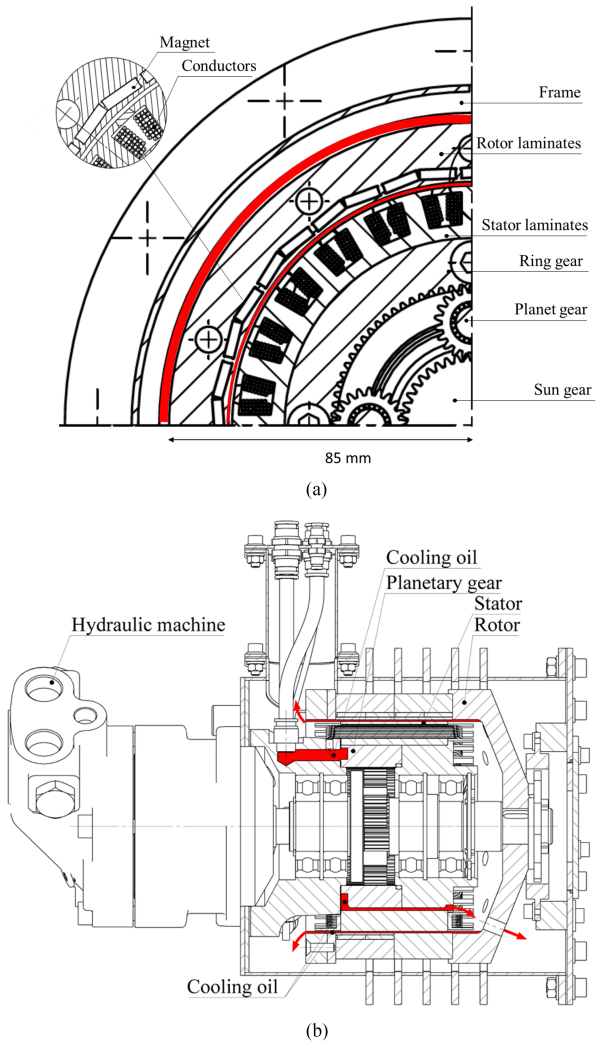

Fig. 1. a) A cross-section from the drive end of the energy converter (oil routes are shown with red color). b) Profile picture of the converter (oil routes with red).

TABLE I
Dimensions and Parameters of the Device

Motor parameters	**24-slot-20-pole, PMSM**
Rated torque T_N, Nm	22
Rated current I_N, A	16.7
Maxwell average tangential stress σ_{Ftan}, kPa	8.8
Stator phase resistance R_s, Ohm (100 °C)	0.31
R_s with connection cables, Ohm (25 °C)	0.33
Stack (physical) iron length l_{Fe}, mm	75
Stator inner diameter D_{si}, mm	115
Stator external diameter, air gap diameter D_s, mm	147.2
Rotor air gap diameter D_r, mm	149.6
Rotor external diameter D_{re}, mm	170
Air gap δ, mm	1.2
PM height, mm	3
PM width, mm	11
Slot area, mm^2	112
Copper space factor	0.45
Current density, A/mm^2	8.6
The total mass of the converter (motor, pump, gear), kg	31
Efficiency, % immersion cooling	89

TABLE II
PARAMETERS UTILISED IN CFD MODEL

Parameter	Value
Oil	Mobil Aero HF series
Density of oil	870 kg/m^3
The specific heat capacity of oil at constant pressure	2300 J/(kgK)
Thermal conductivity of oil	0.185 W/(m·K)
Oil viscosity presented as a function of temperature	$\mu = (-1.2759 \cdot 10^{-4} T + 0.05213) \frac{\text{kg}}{\text{ms}}$
The specific heat capacity of air at constant pressure	1.005 kJ/(kg K)
Thermal conductivity of air	0.025 W/(m·K)

Fig. 1(a) cross-section and Fig. 1(b) profile and Table I describe the structure of the EH converter. The rotor of the device is fixed to the sun gear of the planetary gear system. The ring gear is mounted inside the stator and respectively planetary carrier is attached to the hydraulic machine. The fluid-tight frame can be partly filled with cooling fluid for both lubrication and heat transfer means. There is a fluid channel between the rotor and the core (inlet height is 9 mm and outlet 8 mm), through which oil flows from drive end areas to non-drive areas.

Each rotor pole is structured using two permanent magnets. Magnets (N48SH) are embedded in a pre-glued rotor laminate stack made of M270-35A. The rotor has a two-step skew of 3 mechanical degrees to reduce torque ripple and mitigate 6th and 12th torque ripple. The steel bridge covering the magnets is 1.1 mm thick to increase the synchronous inductance as the motor must be capable of operating also in field weakening. At the rated 7-kW power and 3000 r/min, the PM motor is designed to have stator and rotor teeth peak flux density of 1.8 T and stator yoke peak flux density of 1.5 T. Such high values were, again, selected to improve the motor torque density and specific power.

III. MOTOR HEAT AND MASS TRANSFER ANALYSIS

A. Numerical Methods

When the motor rotates it whips up oil with air and makes a homogeneous aerosol. This was modelled in steady state with ANSYS CFX 2019 R3 software. The CFD computations are performed for different speeds and powers. The losses are modelled by specifying the heat fluxes on no-slip walls. The casing of the motor is modelled as an adiabatic wall. The bearings are modelled as porous media with the volume porosity of 0.57, permeability of $8 \cdot 10^{-7}$ m^2 and resistance loss coefficient of 730 1/m in the streamwise direction, and permeability of $8 \cdot 10^{-10}$ m^2 and resistance loss coefficient of $7.3 \cdot 10^5$ 1/m in the transverse direction. These values are obtained using the Ergun equation [14].

One operating point is presented in detail to show the numerical values and to visualize the oil flow directions and heat transfer inside the energy converter. In this operation point the rotor speed is 2000 rpm, shaft power is 4.6 kW and total losses are 1106 W. The material parameters utilized in CFD are presented in Table II.

Pressure inlet (1 bar, 33 °C, 1% turbulence intensity) and mass flow outlet (0.8 L/min, 0.0116 kg/s) boundary conditions are used. The interfaces between the stationary and rotating parts are modelled with the frozen rotor approach, which is commonly used in quasi-steady CFD e.g., [15], [16]. The turbulence is modelled with the standard k-epsilon model since it allows using wall functions in the studied complex geometry. This approach is also commonly used, see for example [15], [17].

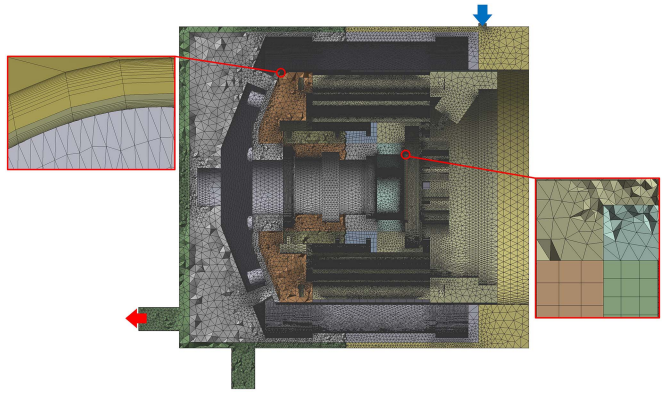

Fig. 2. The computational mesh with the details of the interfaces in the air gap (left) filled with oil aerosol and in the narrow channel between the stator and gear (right). Blue and red arrows present the oil inlet and outlet connections, respectively.

B. Numerical Results

The mesh independent was analysed with four different meshes consisting of 0.2, 1.1, 6.2 and 14.0 million elements. The computational mesh is shown in Fig. 2 with the details of the interfaces in the oil gap and in the narrow channel between the stator and gear.

Structured mesh is used in the air gap and in the narrow channel between the stator and gear, and unstructured mesh elsewhere because of the complexity of the geometry. The results of the mesh independence study are shown in Fig. 3, which presents the pressure loss, oil outlet temperature and maximum oil temperature with respect to the number of mesh elements. The error bars present the discretization error estimated with the Grid Convergence Index method [18].

According to the results of the mesh independence study, the mesh with 1.1 million elements is chosen because there is no significant change in the results with 6.2 million elements, and the results in Fig. 3 indicate that the mesh with 14 million elements is already too dense as the results start to deviate abnormally.

Sometimes refining a mesh too much may lead to errors when simulating at steady state as flow unsteadiness associated with flow separation may only show up once the grid is sufficiently refined [20]. The maximum y+ values occur in the air gap, and the maximum values were 294, 285, 194, and 189 for the meshes from the course to the densest. For the turbulence model with wall functions, the recommended range for the y+ varies from 30 to 300.

The effect of the oil volume fraction was analysed by varying it at the inlet from 0.5 to 0.8. The range was chosen based on the visual estimation during the measurement. This was possible as

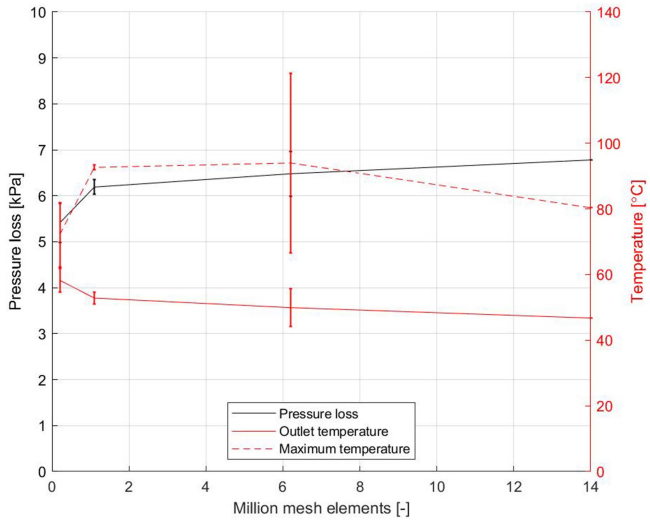

Fig. 3. Mesh independence study using the pressure loss, oil outlet temperature and oil maximum temperature as indicators with respect to the number of mesh elements.

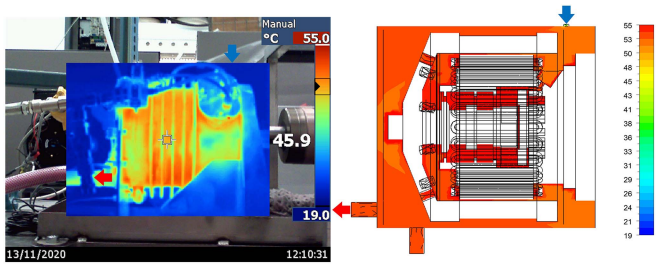

Fig. 4. Measured surface temperature of the motor (left) and the modelled fluid temperature (right, °C). Blue and red arrows show the places of oil inlet and outlet connections, respectively.

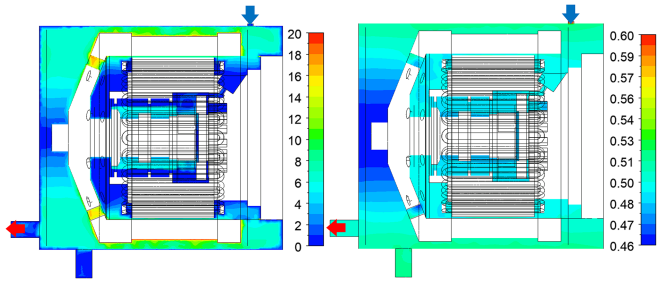

Fig. 5. The contours of absolute velocity (left, m/s) and oil volume fraction (right). Blue and red arrows present the oil inlet and outlet connections, respectively. The highest whipped oil speed (16 …20 m/s) is seen in the holes forming the rotor blower, and on the rotor outer surface.

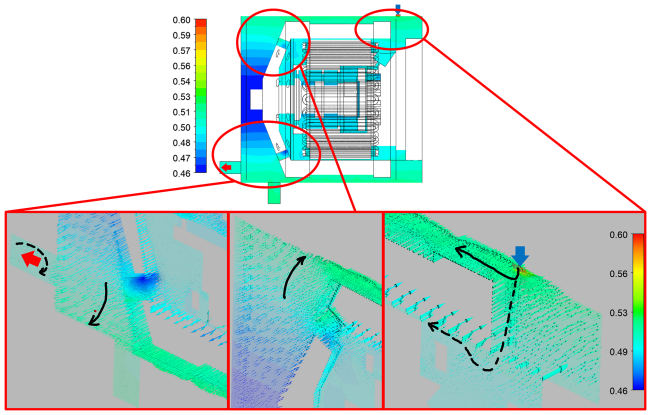

Fig. 6. The velocity vectors near the oil inlet (right), at the air gap outlet (middle), and at the oil outlet (left). The vectors are colored by the oil volume fraction (scale from 0.45 to 0.63), and the solid black arrows indicate the main flow directions, and the dashed black arrows indicate the secondary flow directions.

the back wall of the converter chamber is transparent. When the oil volume fraction at the inlet was changed from 0.5 to 0.6, the modelled oil outlet temperature increased by 5%. When the oil volume fraction was further increased, there was no difference in the oil outlet temperature. Therefore, the oil volume fraction of 0.6 was chosen.

The numerical results are compared to the measured surface temperature of the motor as shown in Fig. 4. The oil outlet temperature measured with a Pt100 sensor was 53 °C matching well with the modelled oil outlet temperature which is also approximately 53 °C. Together with the conducted grid dependency study, the accuracy of the CFD is evaluated to be sufficient for the purpose of this work.

The contours of absolute velocity (Fig. 5) indicate that the oil flows relatively slowly through the stator windings and bearings, but instead it flows faster between the rotor and motor casing.

However, the contours of oil volume fraction (Fig. 5) indicate that there is around 50% air-oil aerosol everywhere in the motor, even in the narrow air gap. The rotation of the rotor tends to throw the oil towards the motor casing due to the centrifugal effect. The rotor drum end-face holes (see e.g., Figs. 4 or 5) also form a centrifugal fan that suck oil from the rotor drum open end towards the fan. Less oil is flowing through the bearings.

The oil flow is mostly affected by the rotating rotor, which can be illustrated with the velocity vectors colored by the oil volume fraction (Fig. 6). The rotation of the rotor tends to suck oil from the inlet to the air gap and between the rotor and the casing (right). At the outlet of the air gap, the vectors colored by the oil volume fraction indicate that the centrifugal effect tends to throw the oil towards the casing from the shaft (middle). As the oil outlet is located horizontally in the axial direction of the motor, the centrifugal effect complicates the outflow of the oil, resulting in a reversed flow at the outlet connection (left). There is also another outlet connection located vertically at the bottom of the motor, but this connection was not used in the experiments, and it is modelled as a wall.

The planes shown in Fig. 7 were created in the computational domain for post-processing purposes to separate the mass flow rates through bearings (green), air gap (blue), windings (orange), and between the casing and rotor (red) from each other. The planes in the middle of the domain were used, and the results are shown in Fig. 8, which indicates that almost half of the flow goes between the casing and rotor or through the windings. Only

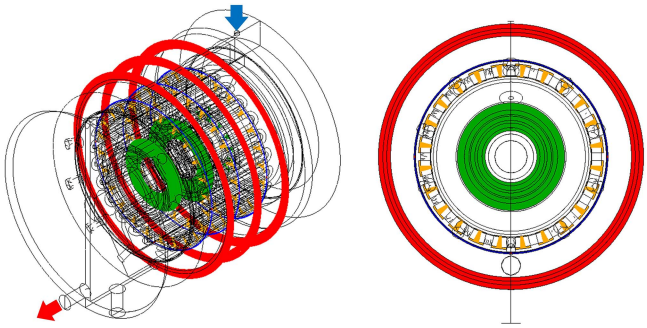

Fig. 7. Planes to separate the mass flow rates through bearings (green), air gap (blue), windings (orange), and between the casing and rotor (red) from each other.

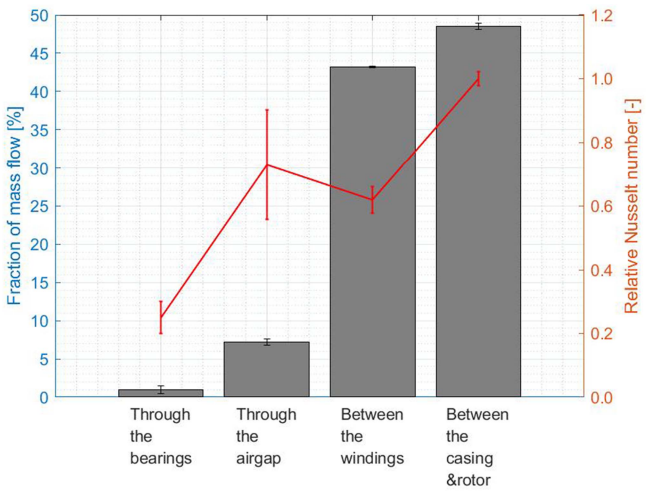

Fig. 8. Fraction of oil mass flow through the bearings, air gap, windings and between the casing and rotor with the error bars of discretization error, and the relative Nusselt number between the casing and rotor with the error bars of discretization error.

approximately 7% of the oil goes through the air gap, and around 1% through the bearings. In addition to mass flows, Fig. 8 shows the Nusselt number relative to that between the casing and rotor. The Nusselt number describes the convection heat transfer at the surface as follows

$$Nu = \frac{hl}{k_{\text{oil}}} \tag{1}$$

$$h = \frac{q''}{(T_{\text{oil,ave}} - T_{\text{surface}})}, \tag{2}$$

where h is the heat transfer coefficient, l of 70 mm is the distance between the inlet and outlet observation planes, q'' is the heat flux, $T_{\text{oil,ave}}$ is the average oil temperature between the inlet and outlet observation planes, and T_{surface} is the maximum surface temperature.

According to the Nusselt number, the most efficient cooling occurs between the casing and rotor. The cooling in the air gap is nearly as efficient as with the oil flowing between the windings even though its mass flow rate is much lower. The cooling is worst in the bearings as only a small fraction of oil flows through them and the surface temperature increases. The discretization error is presented with the error bars.

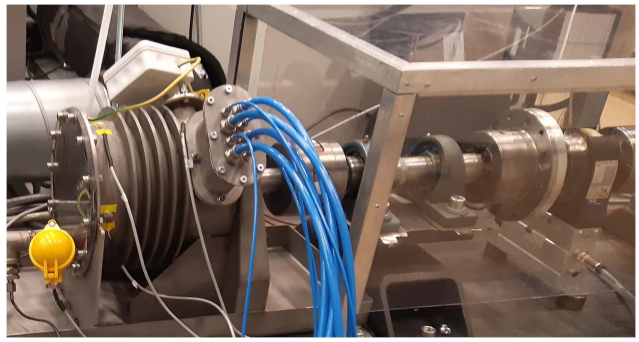

Fig. 9. The EH converter motor (on the left) attached on a test bench.

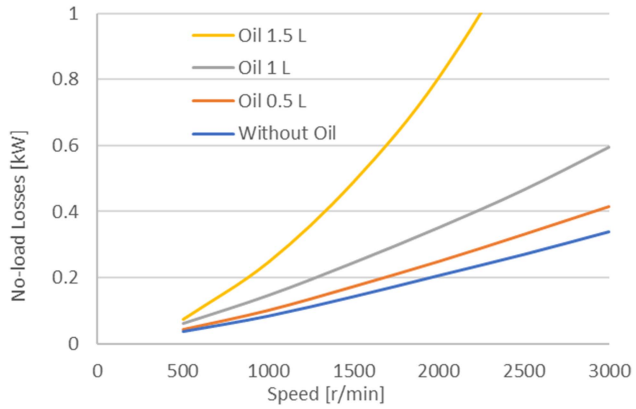

Fig. 10. No-load losses as a function of oil amount in the motor chamber as a function of speed, oil amount as parameter.

IV. Experimental Results

The EH converter motor equipped with the gear was tested separately (without pump unit) in a test bench shown in Fig. 9.

Motor temperatures are measured with Pt-100s, electrical values with Yokogawa PX8000 power analyser and speed/torque with torque transducer.

No-load losses were first measured without heat-transfer oil in the system to get a reference level with no oil drag losses. Then immersion-cooling oil level was increased step by step up to 1.5 litres. Finally, the external oil circuit unit was tested with an oil flow of 0.8 litre/min. The heat-transfer oil increases drag losses, and its effects depend on both the amount and temperature of the coolant. The oil drag force in the air-gap is calculated with Petroff's law [20] to be 80 W at 30 °C oil temperature. The no-load losses are 340 W without oil (see Fig. 14) and when 0.5 litres of oil is added in the motor chamber (immersion cooling) the no-load losses increase to 410 W at the rated speed of 3000 r/min as presented in Fig. 10. Thereby oil-drag losses are 70 W with immersion cooling and 0.5 litre filling. When the oil amount inside the motor chamber is further increased from 0.5 litres to 1 litre, the oil-drag increases to impractical levels. With

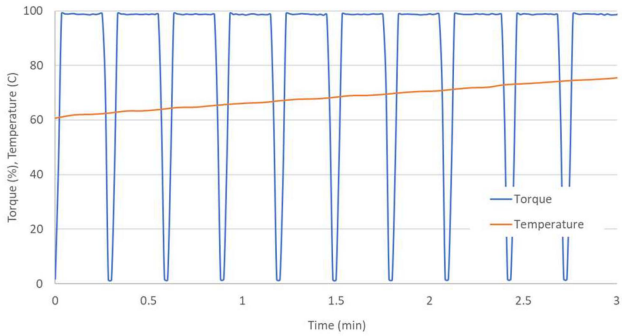

Fig. 11. Immersion cooling. Cyclic load at 3000 rpm 100% torque on and 3 s off time.

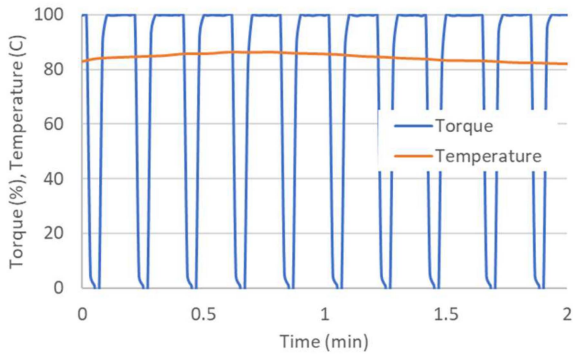

Fig. 12. Oil-flow cooling 0.8 litre/min at cyclic load (80/20) with 100% torque.

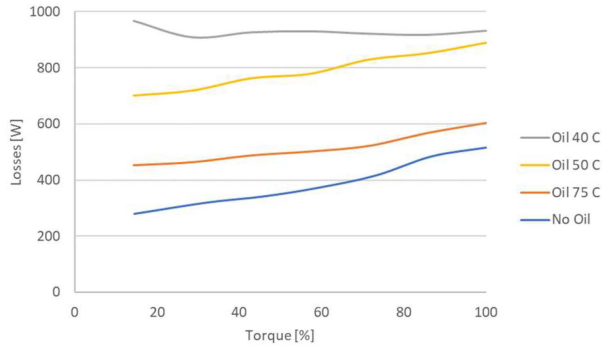

Fig. 13. Motor-gear system losses as a function of torque with no oil flow and with 0.8 L/min oil flow at different oil temperatures at 2000 rpm.

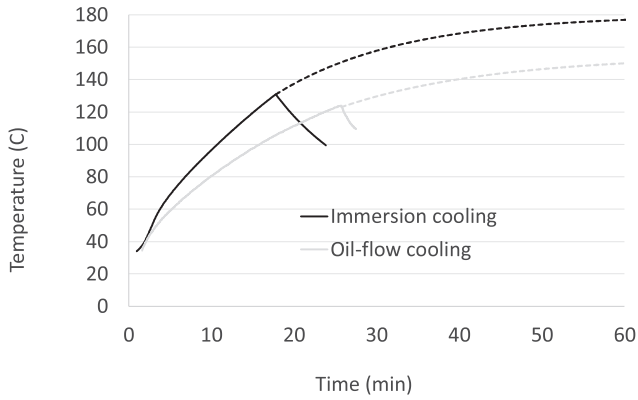

Fig. 14. The temperatures in motor end windings at 7-kW shaft power at 3000 r/min speed with immersion cooling (0.5 litre oil in motor chamber) and with oil-flow cooling (0.8 L/min). Oil input temperature is 33 °C. The time constants to apply (4) are 16 min for immersion cooling and 25 min for oil-flow cooling.

0.8 L/min oil-flow cooling the measured no-load losses are 455 W. This value is slightly higher than with immersion cooling.

Cyclic load tests are carried out to discover how well the motor-gear system can handle typical cyclic loads. The machine with immersion oil cooling is driven at the rated speed of 3000 r/min with 100% torque for 14 s and then 0% torque for 6 s. This driving cycle is repeated until thermal equilibrium is reached. The machine performance meets the definition of 7-kW, S3, 70%.

In another test the off-time was reduced to 3 s. The motor-gear set can be driven at its rated speed and 100% torque on cyclic duty as seen in Fig. 11. This kind of heavy-duty cycle can be repeated for 45 minutes until windings reach 155 °C.

In the next phase, the oil-flow cooling is tested. Measurement results with cyclic duty are presented in Fig. 12, where 100% torque is applied on/off at 2000 rpm speed. It can be seen that the temperature in the windings varies between 82 °C and 86 °C. Moreover, load cycles on 100% torque 80% of the period and rest time 20% keep the temperatures in windings nearly constant from the beginning until the end of the tests.

During the tests with oil-flow cooling the nature of oil with varying viscosity is clearly notable. Electric motor losses are recorded as a function of torque with no oil flow and with 0.8 L/min oil flow at different oil temperatures at 2000 rpm speed. The measured motor losses, depicted in Fig. 13, are small as the flowing oil is warm. Thereby drawing an accurate efficiency map would require steady inlet oil temperature adjustment.

Heat run tests with constant load and speed were also performed in laboratory. The machine is designed for cyclic use and, therefore, steady state heat run is applied only until windings reach temperature of 130 °C. The temperature rise is thereafter extrapolated with time constants and equation [21]

$$\Delta T = \Delta T_{\max}\left(1 - e^{-\frac{t}{\tau}}\right) + \Delta T_0 e^{-\frac{t}{\tau}} \tag{3}$$

where ΔT_0 is the temperature rise over ambient and $\Delta T_{\max}$ is the maximum temperature rise over ambient and τ is the thermal time constant. Fig. 14 depicts the temperature rise in the motor windings at 7-kW power at 3000 r/min speed with immersion cooling (0.5 litres in the chamber) and with liquid cooling (0.8 L/min). The solid lines are from measurements and dotted lines are from (4) using time constants from [21].

A clear difference can be observed between the two cooling approaches. In addition, the operating time at 7-kW load is not sufficient to reach thermal equilibrium. According to the heat run tests with immersion cooling the winding temperature may reach 150 °C when the shaft power is continuously 3.5 kW. Therefore, with this cooling approach, the machine power can be designated at 3.5 kW S1. However, the converter is designed for cyclic loads. From the 7-kW heat test in Fig. 14, one can see,

TABLE III
SHAFT POWER AND WINDING TEMPERATURES IN STEADY STATE

	Immersion cooling (0.5 L oil in motor chamber)		Oil-flow cooling (0.8 L/min, oil input temperature 33 °C)			
Shaft power, kW	3.5	7	3.5	4.6	5.3	7
Speed, rpm	1500	3000	1500	2000	2500	3000
End winding temperature (°C)	150	180*	80	96	105.5	155*

*Final value computed from measured curves.

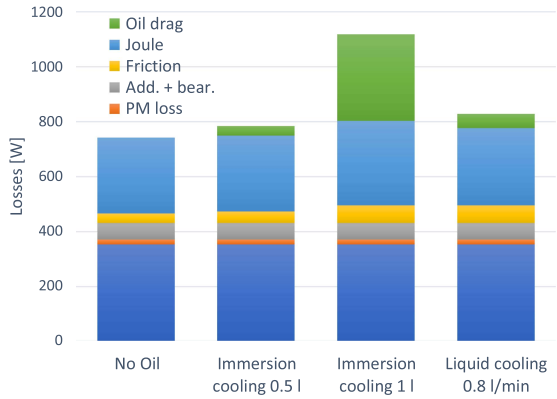

Fig. 15. Loss components of the motor with no heat-transfer oil in the machine, 0.5 and 1 liters heat-transfer oil in the chamber, and 0.8 L/min liquid cooling.

that the machine can operate on cyclic duty S2 20 min. Since it cools fast about 50% duty cycle can be used.

The heat run tests with oil-flow cooling revealed that the energy converter can be utilized in continuous duty S1 at 7-kW. The results in Table III confirms that the end winding temperature does not exceed 155 °C. In comparison, the same operating point with immersion cooling would lead to end winding temperature of 180 °C and thereby the difference of these cooling methods is 25 °C in these laboratory test.

Loss components are segregated with measured values ($3I^2R$, No-load losses), finite element analyse values (iron losses) and analytical equations (mechanical, friction). These loss components are given in Fig. 15 for cases: Without oil, with immersion cooling having heat-transfer oil amount of 0.5 and 1.0 litres in the chamber, and with liquid cooling of 0.8 L/min.

With immersion cooling in this machine, there is a suitable cooling effect when having approx. 0.5 litres of heat-transfer oil in the chamber and the oil drag loss is on a moderate level. The efficiency of the motor is 0.909 without oil and it drops to 0.894 when 0.5 litres oil is added. With 1 litre, the measured oil drag losses are 315 W and friction losses double. In oil-flow cooling when the oil temperature varies during the cycle, the oil drag losses will also vary because of viscosity. With oil-flow cooling the measured losses varied from 830 W to 1050 W.

Nevertheless, the instantaneous total losses with a warm motor are presented in Fig. 16 for a motor without oil and Fig. 17 for a motor with 0.5 litre oil in the chamber and in Fig. 18 with oil-flow cooling. The friction loss with oil-flow cooling (Fig. 18) are high, indicating that the oil level in that case is higher than with 0.5 litre immersion cooling (Fig. 17).

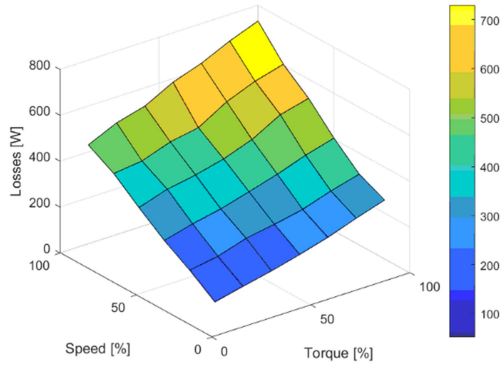

Fig. 16. Losses as a function of speed and torque for a motor without oil.

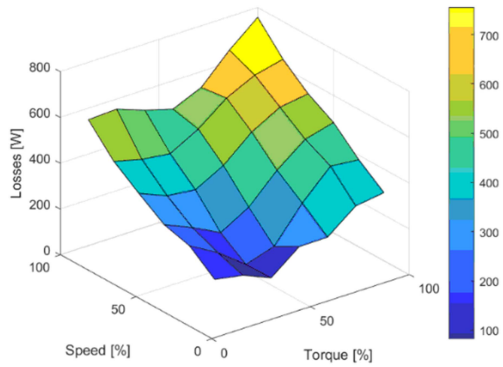

Fig. 17. Losses as a function of speed and torque for immersion cooling with 0.5 litres of oil in the chamber.

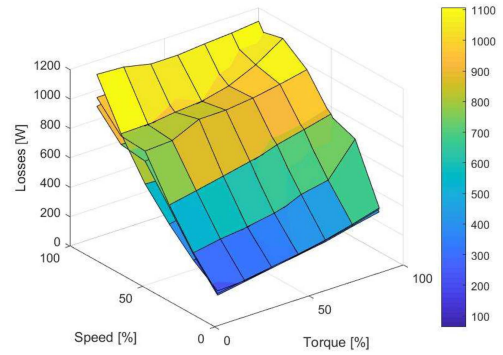

Fig. 18. Losses as a function of speed and torque with oil-flow cooling (0.8 L/min).

Log loader tests: After laboratory tests, the pump is assembled to the motor-gear system and the energy converter is attached to a log loader. The required movements generate a cycle with lifting up-movement, shifting horizontal, laying down the load and in some cases, there is a no-load time before next cycle starts. These cycles are defined as periodic duty cycles S3 – S8 [13]. The operations are tested with 3 different load masses: 201, 439 and 561 kg.

In this test, the recuperated energy can be stored to battery and gain energy savings. Therefore, the required power was measured from the log loader with the designed energy converter. As an example, the recorded shaft power, torque and speed whilst lifting a 439 kg mass, is presented in Fig. 19. From the

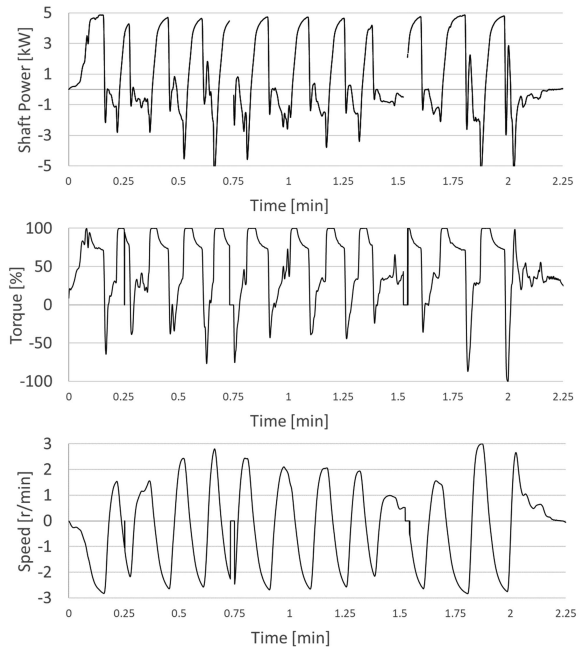

Fig. 19. Power, torque and speed cycles when lifting a 439 kg mass with the energy converter. Torque 100% equals to 66 Nm shaft torque.

TABLE IV
MEASUREMENT RESULTS DURING LOG LOADER CYCLES HAVING IMMERSION COOLINC

Load mass	**201 kg**	**439 kg**	**561 kg**
Aver. Shaft Power [kW]	1.93	2.18	3.92
Consumed energy kWh	4.68	3.36	4.39
Regenerated energy kWh	1.59	1.28	1.59
Energy saving [%]	25	28	27
Average speed [r/min]	1300	1467	2000
Average torque [%]	45.1	57.5	72.3
Winding Temperature, C	62 - 71	52 - 58	61 - 70

curves it can be calculated that there is 28% regenerative braking energy available in the cycle (integrated negative power). From lifting test loads, the energy saving possibilities are collected to Table IV. The energy savings with the tested cycles varied from 25% to 28% as compared to conventional pump system. It is also worth mentioning, that the end winding temperatures remained below 80 degrees during the tests with the log loader.

V. CONCLUSION

An electric motor is designed to be integrated around a planetary gear and attached to a bent-axis hydraulic piston machine. The electrohydraulic converter is cooled by 1) using a suitable amount of heat-transfer oil inside the motor chamber and 2) oil flowing through the machine.

The oil-flow routes, and the cooling efficiency were numerically studied. It was shown that, in the liquid cooling approach, centrifugal effects play a key role, and the majority of oil flow goes through the windings and through the channel between the casing and the rotor. However, despite of the problems with a very low flow rate in the air gap, the heat transfer is reasonably efficient in that area.

Measurements are first performed for the motor and gear system in a laboratory test bench and later the whole converter is driven in a real test case, in a log-loader machine, and the designed EH converter fulfilled well the requirements. Energy savings up to 28% in log loader cycle can be achieved according to measurements. The designed EH energy converter with immersion cooling performs well in periodic duty cycles and with oil flow cooling it suits for continuous running duty cycle following the motor label S1, 7-kW.

The oil-flow cooled option is therefore too powerful for the test case log loader. It can handle more demanding load cycles. For this log loader cycle, immersion cooling is an excellent option, and it suits well for other cyclic duties.

REFERENCES

[1] Make Transport Greener - European Commission, ISBN 978-92-76-39643-7, doi: 10.2775/421628.1.7.2021.
[2] O. A. Lysenko and A. V. Simakov, "The pump hydraulic load effect determination on the parameters of an frequency-controlled asynchronous electric drive," in *Proc. IEEE Dyn. Syst., Mechanisms Machines (Dyn.)*, 2019, pp. 1–6.
[3] Y. Noh, W. Kim, and J. Lee, "Online short-circuit protection strategy of an electric powerpack for electric oil pump applications," *IEEE Access*, vol. 9, pp. 52292–52309, 2021.
[4] Q. Xun, Y. Liu, X. Huang, E. A. Grunditz, J. Zhao, and N. Zhao, "Drive cycle energy efficiency of fuel cell/supercapacitor passive hybrid vehicle system," *IEEE Trans. Ind. Appl.*, vol. 57, no. 1, pp. 894–903, Jan./Feb. 2021.
[5] P. Ponomarev, R. Åman, H. Handroos, P. Immonen, J. Pyrhönen, and L. Laurila, "High power density integrated electro-hydraulic energy converter for heavy hybrid off-highway working vehicles," *IET Elect. Syst. Transp.*, vol. 4, no. 4, pp. 114–121, 2014.
[6] A. Khamitov, J. Swanson, J. Van de Ven, and E. L. Severson, "Modeling, design, and testing of a linear electric-hydraulic conversion machine for electrification of off-highway vehicles," *IEEE Trans. Ind. Appl.*, vol. 57, no. 3, pp. 2449–2459, May/Jun. 2021.
[7] F. Nishanth, G. Bohach, J. V. de Ven, and E. L. Severson, "Design of a highly integrated electric-hydraulic machine for electrifying off-highway vehicles," in *Proc. IEEE Energy Convers. Congr. Expo* ., 2019, pp. 3983–3990.
[8] H. Moradisizkoohi, N. Elsayad, and O. A. Mohammed, "Experimental verification of a double-input soft-switched DC–DC converter for fuel cell electric vehicle with hybrid energy storage system," *IEEE Trans. Ind. Appl.*, vol. 55, no. 6, pp. 6451–6465, Nov./Dec. 2019.
[9] L. Callaghan and S. Lynch, "Analysis of electric drive technologies for transit applications: Battery-electric, hybrid-electric and fuel cells," Northeast Advanced Vehicle Consortium, Boston, MA, USA, Rep. FTA-MA-26-7100-05.1, 2005.
[10] H. Morr, "Transient thermal analysis with verified simplications on a newly designed compact electrohydraulic energy," *Intership Rep.*, 2020.
[11] P. Lindh, C. Di, L. Laurila, E. Scherman, H. Handroos, and J. Pyrhönen, "Compact electrohydraulic energy converter for off-road machines," in *Proc. IEEE Int. Electric Machines Drives Conf* ., 2021, 1–5.
[12] J. Pyrhönen, T. Jokinen, and V. Hrabovcova, *Design of Rotating Electrical Machines*. Wiley, 2008.
[13] IEC 60034-1 Duty Cycles of Operating Electrical Motors, 2013. [Online]. Available: https://avsld.com.sg/iec-duty-cycles/
[14] S. Ergun, "Fluid flow through packed columns," *Chem. Eng. Prog.*, vol. 48, no. 2, pp. 89–94, 1952.
[15] K. Bersch, P. H. Connor, C. N. Eastwick, and M. Galea, "CFD and experimental investigation into a non-intrusive method for measuring cooling air mass flow rate through a synchronous generator," *J. Eng.*, vol. 2019, no. 17, pp. 4432–4435, 2019.
[16] A. Rasekh, P. Sergeant, and J. Vierendeels, "Fully predictive heat transfer coefficient modeling of an axial flux permanent magnet synchronous machine with geometrical parameters of the magnets," *Appl. Thermal Eng.*, vol. 110, pp. 1343–1357, 2017.

[17] X. Fan, R. Qu, J. Li, D. Li, B. Zhang, and C. Wang, "Ventilation and thermal improvement of radial forced air-cooled FSCW permanent magnet synchronous wind generators," *IEEE Trans. Ind. Appl.*, vol. 53, no. 4, pp. 3447–3456, Jul./Aug. 2017.
[18] I. Celik et al., "Procedure for estimation and reporting of uncertainty due to discretization in CFD applications," *J. Fluids Eng.*, vol. 130, no. 7, 2008, Art. no. 078001, doi: 10.1115/1.2960953.
[19] F. P. Incropera et al., *Fundamentals of Heat and Mass Transfer*, 6th ed. Hoboken, NJ, USA: Wiley. 2007, Art. no. 997.
[20] J. H. Ferziger, M. Perić, and R. L. Street, *Computational Methods for Fluid Dynamics*, 4th ed. Cham, Switzerland: Springer, 2020, Art. no. 596.
[21] K. Woronowicz, A. Safaee, and A. Maknouninejad, "Enhanced algorithm for real time temperature rise prediction of a traction linear induction motor," in *Proc. IEEE Transp. Electrific. Conf. Expo* ., 2018, pp. 616–620.
[22] P. Ponomarev, "Tooth-coil permanent magnet synchronous machine design for special applications," Ph.D. dissertation, Lappeenranta Univ. of Technology, Lappeenranta, Finland, 2013.

Pia Lindh (Senior Member, IEEE) was born in Helsinki, Finland, in 1969. She received the M.Sc. degree in energy technology and the D.Sc. degree in electrical engineering (technology) from the Lappeenranta University of Technology (LUT), Lappeenranta, Finland, in 1998 and 2004, respectively. She is currently an Associate Professor with the Department of Electrical Engineering, LUT Energy, Lappeenranta, where she is engaged in teaching and research of electric motors and electric drives. Her research interests include electrical machines, especially permanent magnet machines and drives.

Jonna Tiainen received the D.Sc. degree in technology from the Lappeenranta University of Technology (LUT), Lappeenranta, Finland, in 2018. Since 2018, she has been a Postdoctoral Researcher with LUT. Her research interests include turbomachinery and interested in developing energy storage technologies. She has gained expertise in CFD and flow-field measurements. Currently, she is studying cavitation of cryogenic fluids.

Aki Grönman, received the doctoral degree from the Lappeenranta University of Technology (LUT), Lappeenranta, Finland, in 2010. He was a Visiting Researcher with the Leibniz University of Hannover, Hanover, Germany, in 2008 and with the University of Stuttgart, Stuttgart, Germany, in 2012. Since 2014, he has been an Associate Professor with the Research Group of Computational Fluid Dynamic, LUT. His main research interests include turbine and compressor aerodynamics and design with special interest in renewable energy production. In turbines, he has concentrated on subsonic, transonic, and supersonic designs with ideal and real gases including both wet and dry flows. Whereas, in centrifugal compressors the conducted research has been dealing with subsonic designs including both diffuser and impeller studies. The first objective of his research is to improve the performance of turbomachinery by better fundamental understanding of the internal flows in turbines and compressors and second branch is to combine different fields of science to solve both global and local energy related problems.

Teemu Turunen-Saaresti received the D.Sc. degree from the Lappeenranta University of Technology (LUT), Lappeenranta, Finland, in 2004. He is currently a Professor of fluid mechanics dynamics with LUT and the Head of the Research Group, Laboratory of Fluid Dynamics. His main research interests include supercritical fluids and power cycles, heat pumps, organic Rrankine cycles, turbomachinery, and computational fluid dynamic. In addition, he is active in research of hydrogen compression.

Chong Di was born in Wuxi, China, in 1991. He received the B.Eng. and M. Eng. degrees in electrical engineering from the Hefei University of Technology, Hefei, China, in 2014 and 2017, respectively, and the D.Sc. degree in technology from the Department of Electrical Engineering, Lappeenranta University of Technology, Lappeenranta, Finland, in 2021. Since 2022, he has been a Lecturer with the Hefei University of Technology. His research focuses on high-speed electrical machines.

Lasse Laurila was born in Helsinki, Finland, in 1971. He received the M.Sc., Lic.Tech., and D.Sc. degrees from the Lappeenranta University of Technology, Lappeenranta, Finland, in 1996, 2000, and 2004, respectively. He is currently an Associate Professor with the Laboratory of Electrical Drives Technology, Lappeenranta University of Technology. His research interests include power electronic converters, variable-speed drives and their control. He is currently research focuses on energy-efficient mobile electric drives.

Eero Scherman was born in Lappeenranta, Finland, in 1987. He received the B.Eng. degree in mechanical engineering from the Saimaa University of Applied Science, Lappeenranta, Finland, in 2011, and the M.Sc. degree in 2020. His main research focuses on development of mechanical engineering in electric motors and generators.

Heikki Handroos (Member, IEEE) received the M.Sc. (Eng.) and D.Sc. (Tech.) degrees from the Tampere University of Technology, Tampere, Finland, in 1985 and 1991, respectively. Since 1992, he has been a Professor of machine automation with the Lappeenranta University of Technology, Lappeenranta, Finland. He has been a Visiting Professor with the University of Minnesota, Minneapolis, MN, USA, Peter the Great St. Petersburg Polytechnic University, Saint Petersburg, Russia, and the National Defense Academy, Yokosuka, Japan. He has authored or coauthored about 300 international scientific papers and supervised about 28 D.Sc. (Tech.) theses. His research interests include modeling, design, and control of mechatronic transmissions to robotics and virtual engineering. He has been an Associate Editor for *ASME Journal of Dynamic Systems, Measurement and Control*, since 2014. He has led several important domestic and international research projects.

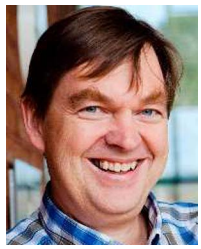

Juha Pyrhönen (Senior Member, IEEE) was born in Kuusankoski, Finland, in 1957. He received the D.Sc. degree in electrical engineering from the Lappeenranta University of Technology (LUT), Lappeenranta, Finland, in 1991. In 1997, he became a Professor of electrical machines and drives at LUT. He is engaged in research and development of electric motors and power-electronic-controlled drives. Prof. Pyrhönen has wide experience in the research and development of special electric drives for distributed power production, traction drives, high-speed applications, permanent magnet materials and applying them in machines have. Currently, he is also researching new carbon-based materials for electrical machines.